arXiv:2609.25900v1 [cs.RO] 22 Sep 2026

You Should Be Properly Scoring Your Odometry

Ola Rønning[1], Usama Saqib[1], and Andrzej Wąsowski[1]

***Abstract*— When we evaluate the performance of our odometry, it is common practice to score the estimated track against a ground truth. Unfortunately, scoring uses point metrics, such as the root mean square error, that ignore the covariance matrix which estimators like filters and smoothers already report. Using the covariance matters for two reasons. First, the covariance encodes the estimator's uncertainty, so it tells us whether the estimator trusts its own output. An overconfident estimator will not report itself lost. Second, the covariance weights the error in each direction of the estimate. Without the covariance, an estimator is unduly penalized for a high error in an uncertain direction. Instead of point metrics, we should use strictly proper scoring rules. These rules score the estimate together with its reported uncertainty. Strictly proper scoring rules recover the point metrics when no covariance is reported, and they diagnose covariance inconsistency when covariance is reported. Using a one-sided pairwise test, we show that two estimators can expose overconfidence in at least one of them without a ground truth. Strictly proper scoring rules and our pairwise test are available in our open-source framework `smfeval`. As a case study, we use `smfeval` to assess the uncertainty quality of the translational component of ground-based LiDAR-inertial odometry. Across four filters we find overconfidence – the worst case reports centimeter certainty with kilometer error. Knowing the filters are overconfident, we investigate the mechanism. The investigation traces overconfidence to filters crediting LiDAR measurements with more new information than they carry.**

I. Introduction

Odometry methods, such as filters and smoothers, estimate a *belief* over vehicle positions. Unfortunately, standard practice for *evaluating* odometry methods disregards beliefs. First, each belief is reduced to a single point estimate of the position, and the position error is quantified by Euclidean distance of that single point from the ground truth. Second, the resulting sequence of errors is reduced to a single score by taking their average. Uncertainty in that average is typically reported as if the errors were independent. Both these reductions discard covariance, though of different kinds.

The Euclidean distance ignores the covariance of beliefs across the dimensions of a position. That covariance determines the shape of the volume within which we expect to find the vehicle. Under the Euclidean distance, the volume is treated as a sphere, so an error along a direction of high uncertainty is penalized just as strongly as one in a direction where the model is less confident (low uncertainty). Meanwhile, consecutive errors are correlated, as consecutive ground truth and estimated track positions are correlated. Treating them as independent narrows the bars on the reported error score. This narrowing can make statistically indistinguishable methods look distinct and end up ranked. For a physical system, this may also mean that errors are wrongly estimated, often underestimated.

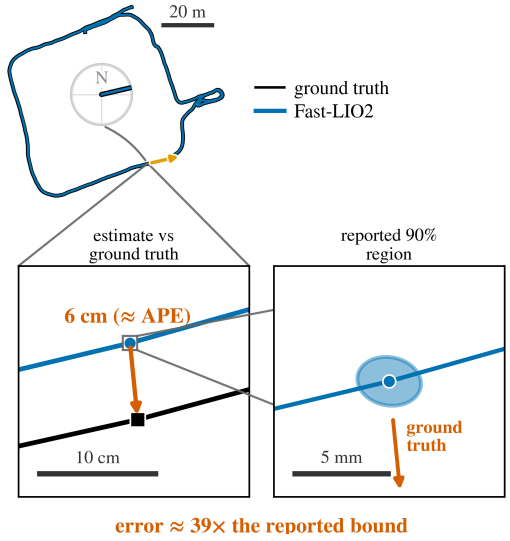

Fig. 1. Error against reported certainty for Fast-LIO2 on the Oxford Spires track keble-college-02.

Gneiting and Raftery [1] define *strictly proper scoring rules* for scoring reported beliefs against an observed outcome in general. Under these rules, the expected score is best only if the belief is consistent with the distribution of outcomes. A single outcome may score well by chance; only considering many outcomes allows us to identify a matching belief (a win), and penalize beliefs too wide or too narrow (a loss). In this work, we apply the strictly proper scoring rules to odometry evaluation. For track estimation, the outcome at each time step is the reference position, so an odometry method is rewarded for assigning uncertainty that matches the errors it makes.

Crucially, the reference (often designated as ground truth) is *itself a measurement* and carries *uncertainty of its own*. Despite this, popular published datasets present it as a point trajectory, so its uncertainty cannot enter the score. As a result every odometry method is judged against a reference that is more certain than it truly is. To emphasize the uncertainty of the reference, we use the term *gold standard* for the reference distribution, reserving the term *ground truth* for single point estimates.

Once the individual positions are scored, the track score is typically defined as their average. This is not a problem in itself, but standard tools, such as `evo` [2], report too narrow error bars because they treat scores as independent. Instead, we propose to use the block bootstrap [3], which resamples contiguous stretches of the track so that temporal dependence

[1]Authors are with Software Quality Research Group, IT University of Copenhagen, Denmark. {oroe,usamas,wasowski}@itu.dk

is preserved. The block length is chosen to capture the range of dependencies in the sequence of scores [4]. The resulting error bars are then correctly widened.

We apply the above evaluation methodology to four LiDAR-inertial odometry filters on ground-based vehicles. Scoring the beliefs properly shows that the filters are overconfident. In the easy setting, the filters report millimeter certainty and err by centimeters (Fig. 1). In the hard setting, reported uncertainty widens to centimeters, but every filter diverges on at least 21 of 55 tracks, and the runs that converge err by decimeters. The worst case, an urban tunnel, pairs centimeter certainty with kilometer error (Fig. 2). Sweeping the configuration parameters traces the overconfidence to the update step of the filters. The same sweep also reveals that the covariance is set by the configuration, not by the residuals. The covariance a planner or fusion node consumes is therefore decoupled from the surroundings, and a vehicle depending on these filters cannot tell that it is lost.

The paper makes the following contributions:

- A proposal of a methodology for properly scoring odometry track estimations, treating uncertainty as first-class, based on the rules of Gneiting and Raftery [1].
- A case study of four LiDAR-inertial odometry filters. We test 67 tracks spanning a feature-rich and a degenerate dataset. The study finds that the reported covariances are 2 to 7 orders of magnitude too tight. A parameter sweep over fixed tracks traces the tightness to the configuration, showing that the reported covariance is set predominantly by the parameters rather than by the residuals.
- A pairwise overconfidence test (Prop. III.2) based on the disagreement between two filters. It applies wherever a gold standard is unavailable or itself uncertain, and it is conservative: disagreement beyond what the two covariances allow implies that one filter is overconfident, while agreement is inconclusive.
- An open-source framework (`github.com/svendbot/smfeval`) that implements the evaluation procedure of Sect. IV, with proper scoring rules, pairwise tests, block-bootstrap intervals, and the SQUARE storage format for estimator beliefs.

We aim to encourage odometry researchers to consider error beliefs when evaluating methods, raising the assessment standards for research and precision reporting in this field.

II. Related work

Track evaluation is standardized around covariance-free metrics. The TUM RGB-D benchmark established the convention for metrics [5], the `evo` tool [2] computes them, and Zhang and Scaramuzza [6] codified the track alignment and aggregation practice. Zhang and Scaramuzza [7] model the gold-standard track as a continuous-time Gaussian process and recast pose error as a likelihood, but the estimate remains a point with no covariance. What we propose instead is to use proper scoring to measure the accuracy and uncertainty of odometry jointly. We support validation and ranking of methods.

The statistic computed by our gold-standard-free test (Prop. III.2) has appeared twice before. Track-to-track association [8] scores the disagreement between two tracks against their combined covariances to decide whether the tracks share a target. Similarly, solution-separation integrity monitoring [9] compares a position estimate from all measurements against estimates that each exclude one measurement, and flags a fault when they disagree. Both works trust the reported covariances and attribute any disagreements to other causes. We interpret a disagreement as evidence against the reported covariances.

Two known effects could explain the overconfidence in our case study (Sect. IV), but do not. First, an extended Kalman filter linearizes at the estimate rather than the truth, so each update shrinks the covariance slightly along directions the measurements do not observe, until after hundreds of updates the covariance no longer covers the error [10]. The filters we use are already far too tight after a single update. Second, the closed-form covariance of point-to-plane registration [11] understates the error [12] because an error shared by all points of a scan, such as a calibration bias, averages away under the independent-noise assumption. We test this directly by integrating such a shared offset out of the likelihood. Doing so recovers only a small fraction of the gap.

III. Scoring position belief

We first recall the classic single point error definition. At each scan $i \in \{1, \dots, n\}$ the estimator reports a position $\hat{t}_i \in \mathbb{R}^3$ and the gold standard supplies t_i. After SE(3) alignment of the two tracks, the position error is the residual $e_i = \hat{t}_i - t_i$, and its Euclidean norm is the absolute pose error (APE). The track score based on APE is classically defined as the root mean square error (RMSE) or the mean absolute error (MAE).

$$\mathrm{RMSE} = \sqrt{\tfrac{1}{n}\textstyle\sum_{i=1}^{n}\|e_i\|_2^2}, \quad \mathrm{MAE} = \tfrac{1}{n}\textstyle\sum_{i=1}^{n}\|e_i\|_2.$$

Consider an example of a robot traveling along a line with an error of $2\,\mathrm{cm}$ for three consecutive scans, so $\mathrm{RMSE} = \mathrm{MAE} = 2\,\mathrm{cm}$. Note that these summaries are the same for estimators that report variance of $4\,\mathrm{cm}^2$ for each scan (consistent with the position error) and $4\,\mathrm{mm}^2$ (far from it).

The alternative to APE is the relative pose error. This error localizes drift within the track by the position error over a window of Δ scans, $e_i^{\Delta} = (\hat{t}_{i+\Delta} - \hat{t}_i) - (t_{i+\Delta} - t_i)$ [5]. The rules of this section apply unchanged for e_i^{Δ} instead of e_i, if the estimator reports a covariance over $\hat{t}_{i+\Delta} - \hat{t}_i$.

A. Proper scoring

Estimators, like filters and smoothers, report a distribution Q over the position, known as its belief, for instance, for a Kalman filter $Q = \mathcal{N}(\hat{t}, \Sigma)$. A scoring rule $S(Q, t)$ assigns the estimator belief a score given that the gold standard reports t for the same scan. The rule $S(Q, t)$ is *proper* when no belief scores better, in expectation, than the reference distribution $t \sim P$ of the gold standard,

$$\mathbb{E}_{t\sim P}[\,S(P,t)] \le \mathbb{E}_{t\sim P}[\,S(Q,t)] \quad \text{for every belief } Q, \quad (1)$$

and *strictly proper* when equality above forces that $Q = P$ [1].

Note that being proper recognizes that the gold standard carries uncertainty itself (otherwise the requirement is vacuous). But being proper is not enough. Consider the scoring

rule assigning the score $S(Q,t) = \|\hat{t} - t\|^2$ to position t with $\hat{t}$ the belief mean (this is the non-aggregated core of RMSE). The rule is proper because it is minimized by $\hat{t} = \mu_P$ (cf. (1)). But this is true for *any* belief with the correct mean. A *strictly proper* rule enforces that the truthful belief is the *unique* minimizer, so any distortion, an inconsistent covariance included, strictly raises the expected score. We advocate strictly proper rules. (Hereafter we write *proper* meaning *strictly proper*.)

Distance-sensitive proper rules: A distance-sensitive rule scores the belief by how far its probability mass lies from the gold standard. A narrow belief close to the gold standard scores better than one far away. Consider the energy score as an example,

$$\mathrm{ES}_\beta(Q,t) = \mathbb{E}_{X\sim Q}[\,\|X-t\|_2^\beta] - \tfrac{1}{2}\,\mathbb{E}_{X,X'\overset{\text{iid}}{\sim}Q}[\,\|X-X'\|_2^\beta],$$

which is strictly proper for $\beta \in (0,2)$ whenever Q has a finite mean [1]. We write ES, if $\beta = 1$. The second term of the energy score discounts the spread the belief reports, so hedging with an inflated covariance is penalized. The energy score recovers the APE if $\beta = 1$ and $\mathrm{Cov}(Q)$ approaches zero [1]. For our example of a robot moving along a line, the honest reported belief variance ($4\,\mathrm{cm}^2$) is scored $1.20\,\mathrm{cm}$ per scan and wins with the overconfident variance of $4\,\mathrm{mm}^2$ that receives a score of $1.89\,\mathrm{cm}$. But as covariance $\mathrm{Cov}(Q)$ approaches zero, the score concentrates near APE, making tight covariances hard to rank with ES. Instead, we need a scoring that diverges as the covariance shrinks, so that tight beliefs remain distinguishable.

Density-based proper rules: A density-based rule instead consults the density the belief assigns to the gold standard itself. Essentially the only density-based rule [13] is the logarithmic score. For a belief Q with density q, we have

$$\mathrm{LogS}(Q,t) = -\log q(t).$$

The score is measured in *nats*. A belief scores one *nat* lower than another when it assigns e times the density to the gold standard. In our example, the honest belief receives 2.1 nats per scan and the overconfident one receives 49. Where the energy score separated the two beliefs by half, the log score separates them by a factor of over twenty. Now, understating the covariance drives the density at the gold standard toward zero and the score becomes arbitrarily large.

Log score of a Gaussian belief: Many Kalman filter variants emit Gaussian beliefs $\mathcal{N}(\hat{t},\Sigma)$, for which the log score splits into

$$-\log q(t) = \tfrac{1}{2}\,(\underbrace{\|e\|_\Sigma^2}_{\text{consistency}} + \underbrace{\log\det\Sigma}_{\text{sharpness}}) + \tfrac{3}{2}\log 2\pi. \quad (2)$$

The consistency term is the square of the Mahalanobis distance $\|e\|_\Sigma = (e^\top\Sigma^{-1}e)^{1/2}$, also called normalized estimation error squared (NEES), a standard consistency statistic [14], and $e = \hat{t} - t$ is the difference from the belief mean, like above. The consistency term penalizes a centimeter of error along an axis where the belief reports millimeters. When the error is zero-mean and the reported covariance is the true error covariance, the scaled error is standard normal and the NEES follows a χ^2_3 distribution, however sharp the belief is. The sharpness term measures how concentrated, i.e., peaked, the belief is [15]. We call $-\log\det\Sigma$ the *reported precision*, the log of the generalized precision $\det\Sigma^{-1}$.

The log score penalizes consistency linearly and sharpness logarithmically. We see this clearly in our example. The errors are $2\,\mathrm{cm}$ and the scalar constant is $\frac{1}{2}\log 2\pi \approx 0.9$. The honest $4\,\mathrm{cm}^2$ belief scores 0.5 nats of consistency and 0.7 of sharpness, recovering the 2.1 per scan (see above). The overconfident $4\,\mathrm{mm}^2$ belief drops sharpness to -1.6 nats, but increases consistency by 50. So the hundredfold decrease in reported variance is penalized heavily because of the asymmetry between sharpness and consistency.

Consistency and sharpness depend on different degrees of freedom of Σ. Write $\Sigma = U\Lambda U^\top$ with U orthogonal and $\Lambda = \mathrm{diag}(\lambda_1,\lambda_2,\lambda_3)$, so that the 1-$\sigma$ ellipsoid of $\mathcal{N}(\hat{t},\Sigma)$ has axes along the columns of U with lengths $\sqrt{\lambda_i}$. We call $(\det\Sigma)^{1/3}$ the scale of Σ, and the axis directions U together with the normalized lengths $\Lambda/(\det\Sigma)^{1/3}$ its shape. Rescaling $\Sigma \mapsto c\Sigma$ multiplies the scale by c and leaves the shape fixed. The following proposition makes the asymmetry exact.

Proposition III.1 (Scaling law of the Gaussian log score)**.** *Let Σ be a 3×3 covariance, $e \in \mathbb{R}^3$ be a fixed error, $c > 0$, and $s = 3\ln(1/c)$. Then*
(i) $\|e\|_{c\Sigma}^2 = \frac{1}{c}\|e\|_\Sigma^2$ and $\log\det(c\Sigma) = \log\det\Sigma - s$.
(ii) The log score (2) of $\mathcal{N}(\hat{t},c\Sigma)$ is

$$\mathrm{LogS}(s) = \tfrac{1}{2}\,\|e\|_\Sigma^2\, e^{s/3} - \tfrac{s}{2} + C, \quad (3)$$

with $C = \frac{1}{2}\log\det\Sigma + \frac{3}{2}\log 2\pi$ collecting the terms free of s. Its derivative $\mathrm{d}\,\mathrm{LogS}/\mathrm{d}s = (\|e\|_{c\Sigma}^2 - 3)/6$ changes sign once, so $\mathrm{LogS}(s)$ has a unique minimum, at $\|e\|_{c\Sigma}^2 = 3$.
(iii) If $\Sigma_e = \mathbb{E}[ee^\top]$ is positive definite, let $A = \Sigma^{-1}\Sigma_e$ and define the shape penalty

$$\psi(\Sigma) = \frac{\mathrm{tr}\,A}{3\,(\det A)^{1/3}} \geq 1, \quad (4)$$

with equality if and only if Σ is a scalar multiple of Σ_e. Then $\mathbb{E}\|e\|_\Sigma^2 = \mathrm{tr}\,A = 3\psi(\Sigma)\,(\det\Sigma_e/\det\Sigma)^{1/3}$, and $\psi(c\Sigma) = \psi(\Sigma)$ for every $c > 0$.

Proof. (i) is $(c\Sigma)^{-1} = \Sigma^{-1}/c$ and $\det(c\Sigma) = c^3\det\Sigma$. (ii) substitutes (i) into (2) and differentiates in s. (iii) is the inequality between the arithmetic and the geometric mean of the three eigenvalues of A, which are positive, and $\psi(c\Sigma) = \psi(\Sigma)$ because $\Sigma \mapsto c\Sigma$ sends $A \mapsto A/c$, so that $\mathrm{tr}\,A \mapsto \mathrm{tr}\,A/c$ and $(\det A)^{1/3} \mapsto (\det A)^{1/3}/c$, and the factor $1/c$ cancels in (4). □

Any belief can be made consistent by scaling, but a consistent belief cannot be made sharper by scaling. By (i), rescaling Σ by c divides the NEES by c, so some c brings $\mathbb{E}\|e\|_\Sigma^2$ to 3 whatever the shape of Σ. Setting $\mathbb{E}\|e\|_\Sigma^2 = 3$ in (iii) gives $\det\Sigma = \psi^3\det\Sigma_e$, and since any other c breaks consistency, this is the sharpness of the consistent belief. Consistency thus fixes the scale of Σ and says nothing about its shape, which the NEES does not measure.

Inflation: The *inflation*

$$k = \frac{\operatorname{med}(\|e\|_{\Sigma}^2)}{\operatorname{med}(\chi_3^2)} \tag{5}$$

is the factor by which the reported covariance must be scaled for the median NEES to reach its calibrated value $\operatorname{med}(\chi_3^2) \approx 2.37$; a consistent filter has $k = 1$. The median makes k insensitive to rare extreme errors that would dominate a mean.

Gold-standard-free overconfidence test: A second estimator can stand in for the gold standard when testing for overconfidence. Let estimators A and B report $(\hat{t}_A, \Sigma_A)$ and $(\hat{t}_B, \Sigma_B)$ for the same scan, with errors e_A and e_B, and write $d = \hat{t}_A - \hat{t}_B = e_A - e_B$ for their disagreement. The *pairwise inflation* is (5) with d in place of e and $\Sigma_A + \Sigma_B$ in place of Σ,

$$k_{\text{pair}} = \frac{\operatorname{med}(\|d\|_{\Sigma_A+\Sigma_B}^2)}{\operatorname{med}(\chi_3^2)}, \tag{6}$$

and measures how far the two reported covariances must be scaled to match the disagreement.

Proposition III.2 (Pairwise overconfidence)**.** *Let the pair A, B have jointly Gaussian, zero-mean errors e_A, e_B with cross-covariance $C_{AB} = \operatorname{Cov}(e_A, e_B)$, and write $M = \Sigma_A + \Sigma_B$ and $V = \operatorname{Cov}(e_A) + \operatorname{Cov}(e_B)$. Let a_X be the largest eigenvalue of $\Sigma_X^{-1/2} \operatorname{Cov}(e_X) \Sigma_X^{-1/2}$ for $X \in \{A, B\}$. Then*
(i) $\operatorname{Cov}(d) = V - (C_{AB} + C_{AB}^\top)$.
(ii) If $\Sigma_A = \operatorname{Cov}(e_A)$, $\Sigma_B = \operatorname{Cov}(e_B)$ *and* $C_{AB} = 0$, *then* $\|d\|_M^2 \sim \chi_3^2$ *and* $k_{\text{pair}} = 1$.
(iii) If $C_{AB} + C_{AB}^\top \succeq 0$, *then* $\max(a_A, a_B) \geq k_{\text{pair}}$*; in particular, if* $k_{\text{pair}} > 1$ *then* $\Sigma_A \succeq \operatorname{Cov}(e_A)$ *and* $\Sigma_B \succeq \operatorname{Cov}(e_B)$ *cannot both hold.*

Proof. (i) follows by expanding $\operatorname{Cov}(e_A - e_B)$. In (ii), $M = \operatorname{Cov}(d)$ by (i), so $M^{-1/2}d$ is standard normal. For (iii), write $a = \max(a_A, a_B)$, so that $\operatorname{Cov}(e_X) \preceq a\Sigma_X$ for both X and $aM \succeq V \succeq \operatorname{Cov}(d)$, the second step by (i) and the hypothesis on C_{AB}. Hence all eigenvalues λ_i of $M^{-1/2} \operatorname{Cov}(d) M^{-1/2}$ satisfy $\lambda_i \leq a$, and $\|d\|_M^2$ is distributed as $\sum_i \lambda_i z_i^2$ with z_i independent standard normal. Since $\sum_i \lambda_i z_i^2 \leq a \sum_i z_i^2$ pointwise and $\sum_i z_i^2 \sim \chi_3^2$, the median of $\|d\|_M^2$ is at most $a \operatorname{med}(\chi_3^2)$, so $k_{\text{pair}} \leq a$. If both estimators are calibrated then $a \leq 1$, giving the particular case. □

Proposition III.2 makes k_{pair} a one-sided test. A value above one, or an interval that excludes one, says that at least one estimator understates its error covariance, but not which one. The bound assumes the two errors are not negatively correlated; error the estimators share, from a common map, sensor or calibration, cancels in d and only makes the test more conservative.

Returning to our example, let two estimators disagree by 2 cm at every scan, one reporting a variance of 1 mm^2 and the other 4 mm^2. The pairwise NEES is 80, against the χ_1^2 median of $\sim$0.455 for scalar positions. The pairwise inflation is $k_{\text{pair}} \approx 176$, so by Prop. III.2 at least one of the two underreports its variance. Had the estimators reported 100 mm^2 and 400 mm^2 instead, the same disagreement gives $k_{\text{pair}} \approx 1.8$, so the test does not detect overconfidence. This, however, does not guarantee calibration, since correlated errors shrink d.

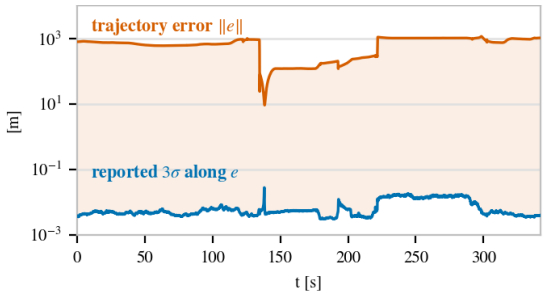

Fig. 2. Error against reported 3σ for I2EKF-LO on GEODE track.

B. Track summaries

All scores discussed so far apply to a single scan, while published benchmarks tend to report per-track summaries. Since position errors are *autocorrelated*, the error at a scan is also correlated with the errors at the scans before it; for example, drift carries over from scan to scan. A track summary is therefore an estimate whose precision rests on how many of the n position errors are effectively independent. Treating all scans as independent overstates the evidence available in the entire track and tends to inflate the certainty of the summary. The *block bootstrap* [3] respects that dependence by resampling contiguous track stretches rather than single scans [16], with a block longer than the correlation length of the errors [4]. The confidence interval is then the spread of the replicates.

Let the per-scan score fluctuate with standard deviation 1 cm and lag-one autocorrelation $\rho = 0.99$, the correlation between the errors of consecutive scans, over a track of $n = 1000$ scans. That autocorrelation gives a correlation length of $(1 + \rho)/(1 - \rho) \approx 200$ scans. With the scans treated as independent, the 95% interval on the track mean is ± 0.06 cm. The autocorrelation inflates the variance of the mean by a factor of 179, so the honest interval is ± 0.83 cm, thirteen times wider.

IV. Case Study: LiDAR-Inertial Odometry

We implement the rules of Sect. III in `smfeval`, an open-source tool that scores an estimator's belief track against a gold-standard track, given either as plain poses or with its own covariance. Beliefs are stored in the SQUARE format, an extension of the TUM track format [5] holding a Gaussian, a weighted particle set, or a plain pose per scan, together with the frame and perturbation conventions the covariance is expressed in.

Using `smfeval`, we investigate four filter-based LiDAR-inertial odometry systems for accuracy and consistency in one easy and one adversarial setting. Oxford Spires [17] is the easy case: feature-rich scenes with distinct geometry to localize against. GEODE [18] is the adversarial case: its tracks are chosen to be degenerate, with symmetric geometry or featureless scenes. A failure on Oxford Spires cannot be attributed to the environment. On GEODE, accuracy is expected to degrade, and the question is whether the reported covariance reveals it.

TABLE I

TRANSLATION ACCURACY AND CONSISTENCY ACROSS FILTERS.

Filter	n	MAE [m] (↓)	Energy [m] (↓)	LogS [nat] (↓)	k (→1)	90% cov (→0.9)
Oxford Spires						
Fast-LIO2	12	**0.088** [0.060, 0.197]	**0.087** [0.059, 0.196]	1×10^{4} $[4, 93]\times10^{3}$	5.6×10^{3} $[2.6, 16]\times10^{3}$	0.000
Faster-LIO	12	**0.117** [0.062, 0.508]	**0.116** [0.061, 0.507]	2.2×10^{4} $[9.1, 690]\times10^{3}$	1.4×10^{4} $[3.9, 480]\times10^{3}$	0.000
Point-LIO	12	0.230 [0.119, 0.481]	0.225 [0.114, 0.475]	$\mathbf{1.5\times10^{3}}$ $[4.8, 86]\times10^{2}$	$\mathbf{5.7\times10^{2}}$ $[1.3, 22]\times10^{2}$	0.000
I2EKF-LO	12	2.37 [0.856, 13.81]	2.37 [0.855, 13.81]	2.3×10^{7} $[3, 580]\times10^{6}$	6.7×10^{6} $[1.3, 240]\times10^{6}$	0.000
GLIM (smoother)	12	0.165 [0.089, 0.314]	–	1.1×10^{2} $[1.4, 35]\times10^{1}$	3×10^{1} $[1.3, 14]\times10^{1}$	0.043
KISS-ICP	12	0.708 [0.312, 1.04]	–	–	–	–
GEODE						
Fast-LIO2	55	7.96 [2.75, 26.05]	7.96 [2.74, 26.05]	8.7×10^{6} $[7.6, 290]\times10^{5}$	2.2×10^{6} $[2.4, 140]\times10^{5}$	0.000
Faster-LIO	55	1.91 [0.708, 24.91]	1.91 [0.706, 24.91]	5.7×10^{5} $[1.4, 300]\times10^{5}$	2.8×10^{5} $[5.5, 2{,}100]\times10^{4}$	0.000
Point-LIO	55	**0.772** [0.407, 31.48]	**0.758** [0.396, 31.47]	$\mathbf{3.3\times10^{3}}$ $[1, 6{,}100]\times10^{3}$	$\mathbf{1.6\times10^{3}}$ $[7.3, 20{,}000]\times10^{2}$	0.000
I2EKF-LO	55	31.45 [14.05, 42.30]	31.44 [14.34, 42.29]	3.5×10^{7} $[1.3, 12]\times10^{7}$	2.3×10^{7} $[5.8, 44]\times10^{6}$	0.000
KISS-ICP	35	9.56 [0.441, 60.89]	–	–	–	–

Experimental setup: From Oxford Spires we evaluate 12 outdoor pedestrian tracks with a LiDAR and an IMU (excluding tracks with known gold-standard problems) against a gold-standard track obtained by registering the LiDAR clouds to a terrestrial laser scanner survey map. From GEODE we evaluate the 55 tracks with a usable gold standard, spanning seven environments and three LiDAR platforms. We benchmark four state-of-the-art filters: the LiDAR-inertial Fast-LIO2 [19], Faster-LIO [20], and Point-LIO [21], and the LiDAR-only I2EKF-LO [22]. We use GLIM [23], at its released defaults, to check whether smoothing over a window of scans, rather than marginalizing each scan, removes the inconsistency. GLIM is a factor-graph smoother and has no per-point R to match, so its k is comparable as a consistency ratio but its inputs are not configured like the filters'. KISS-ICP [24], LiDAR-only, serves as a covariance-free accuracy baseline; our runner reads only `PointCloud2`, so it covers 35 of the 55 GEODE tracks, the 20 absent ones being the Livox-format gamma platform. Beliefs are recorded at scan rate; all four filters use a right-perturbation error state ordered (translation, rotation). We use the dataset-provided filter configurations where available, and the filters' released defaults otherwise. For all filters the measurement noise is fixed to $R = 10^{-3}\,\mathrm{m}^2$ per LiDAR point (Point-LIO $10^{-2}\,\mathrm{m}^2$). We score the absolute translation error. Relative pose error cannot be scored because filters do not report the cross-covariance between poses. We report scores as if the gold standard were exact because neither dataset ships its uncertainty. Using a Gaussian-process interpolation [7], we give it a covariance for the interpolation between gold-standard poses, though not for the survey and registration error behind them, and rescore. This drops NEES by at most $12\,\%$ and changes no findings.

Frames and timing: A scoring rule compares an estimate with a gold-standard position in the same frame at the same time. The extrinsic $E \in \mathrm{SE}(3)$ from the filter's frame to the gold-standard frame multiplies on the right, so the 6×6 covariance transports by the adjoint $\mathrm{Ad}_{E^{-1}}$. Writing J for the translation rows of $\mathrm{Ad}_{E^{-1}}$,

$$\Sigma'_{tt} = J\,\Sigma\,J^{\top}, \qquad J = U^{\top}\begin{bmatrix} I & -\ell^{\wedge} \end{bmatrix}. \tag{7}$$

Here, $U \in \mathrm{SO}(3)$ and $\ell \in \mathbb{R}^3$ are the rotation and lever arm of E. The second block of J carries orientation uncertainty into position through the lever arm; rotating the marginal Σ_{tt} alone would drop that term. Each estimated track is aligned to the gold standard by a whole-track $\mathrm{SE}(3)$ fit; that alignment of world frames multiplies on the left and leaves Σ untouched. From here on, Σ denotes this transported block. For time alignment, each estimate is paired with the gold standard by nearest-neighbor timestamp matching within $5\,\mathrm{ms}$, under a centimeter of motion at walking pace. The Gaussian-process rescoring above also removes this mismatch and does not change the outcome.

A. Every reported covariance is orders of magnitude too tight

Table I reports medians over tracks of per-track values, with 95% bootstrap intervals from resampling tracks. Per track, MAE, ES and LogS are means over scans of the absolute position error, energy score and log score; k is the inflation of (5) computed per track, and coverage $\mathrm{cov}_{0.9}$ is the fraction of scans whose gold-standard position falls inside the reported 90% region. The energy score collapses to MAE as the covariance shrinks, and here it tracks MAE to within two percent. That is itself a symptom. The reported covariances are too small for a distance-sensitive score to register them. Bold marks the best filter and every filter it does not significantly beat by a paired Wilcoxon signed-rank test over the shared tracks, Holm-corrected within each metric at $\alpha = 0.05$. GLIM and KISS-ICP are references and are excluded from the test. Coverage is reported without intervals or bold because it is zero on nearly every track, so intervals collapse and the test does not separate the filters.

Accuracy raises no flags: Point error is well-behaved across the 12 Spires tracks. The per-filter median MAE (Table I) places the three LiDAR-inertial filters within $0.3\,\mathrm{m}$ of the gold standard, an accuracy at which nothing would prompt a closer look. GLIM is comparable at $0.17\,\mathrm{m}$. The covariance-free KISS-ICP trails at $0.71\,\mathrm{m}$, which bounds what LiDAR

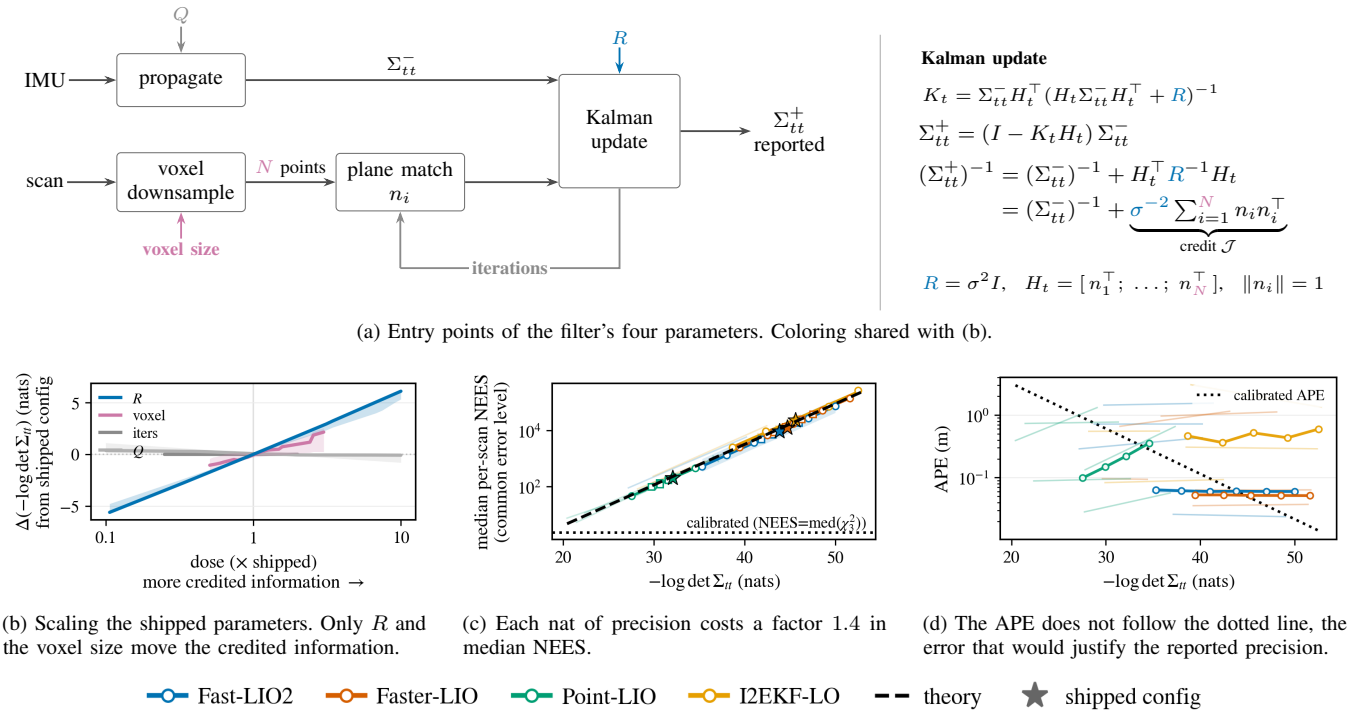

(a) Entry points of the filter's four parameters. Coloring shared with (b).

(b) Scaling the shipped parameters. Only R and the voxel size move the credited information.

(c) Each nat of precision costs a factor 1.4 in median NEES.

(d) The APE does not follow the dotted line, the error that would justify the reported precision.

Fast-LIO2 Faster-LIO Point-LIO I2EKF-LO theory shipped config

Fig. 3. Configuration sweeps of the four filters.

alone achieves here; the LiDAR-only I2EKF-LO falls short of it at 2.4 m. On GEODE the filters diverge (MAE ≥ 5 m) on 21 to 43 of the 55 tracks depending on the filter, as expected from the degenerate geometry; on these tracks the covariance should grow with the error.

The filters are overconfident: Table I shows that the concentration is unwarranted for all four filters. Even the best log score runs to thousands of nats where a consistent filter would score a few. Splitting the Gaussian log score ((2)) into its two terms, the NEES term contributes 10^3–10^7 nats while the sharpness term sits between -45 and -32 nats, so the penalty is almost entirely for inconsistency. The inflation k is between 5.7×10^2 and 6.7×10^6 on Spires, so the reported covariances would have to be scaled up by hundreds to millions to match the errors. A calibrated filter has $\mathrm{cov}_{0.9} = 0.9$, an overconfident one less; here $\mathrm{cov}_{0.9}$ is near zero for every filter, so the reported 90% ellipsoid almost never contains the truth.

Divergence does not explain the overconfidence. Between 12 and 34 of the 55 GEODE tracks converge per filter, with MAE < 5 m; on those alone, median NEES stays at 10^3–10^5 and $\mathrm{cov}_{0.9}$ at zero for every filter.

Scene degeneracy does not explain it either. We measure degeneracy by the condition number $\kappa = \lambda_{\max}/\lambda_{\min}$ of the scan's point-to-plane information $\sum_i n_i n_i^\top$, with n_i the surface normal at point i of the downsampled scan, estimated by principal component analysis. Where the normals concentrate, κ grows, since a translation orthogonal to the normals leaves every point-to-plane residual unchanged and such poses cannot be distinguished. Regressing per-scan $\log\|e\|_\Sigma^2$ on $\log\kappa$ gives $R^2 \leq 0.014$ over one order of magnitude of κ on Spires and 6.6 orders on GEODE, so overconfidence is as severe on well-conditioned scans as on degenerate ones. The same holds for the trace, log-determinant and smallest eigenvalue of the information matrix of the two filters with accessible Jacobians ($R^2 \leq 0.027$). On the same 12 Spires tracks the smoother GLIM, which keeps a window of scans instead of marginalizing each, is far less overconfident at a competitive MAE, $k = 29.7$, yet still inconsistent. The severity in the filters therefore points to what all four share, an iterated error-state Kalman filter [25] with a point-to-plane model against a map treated as exact.

The overconfidence survives without a gold standard: We score the filters against each other. We bring one estimate into the other's frame by a rigid Umeyama fit on their matched translations, so the gold standard never enters. Taking the gauge from the gold-standard alignment instead moves k_{pair} by under 5% on Spires and up to 2× on GEODE, small against k_{pair} itself, so the result does not depend on the gauge. By Prop. III.2, k_{pair} is a lower bound on the larger of the two inflations. We observe $k_{\mathrm{pair}} \approx 180$–$330$ on Spires and 15 to 5.8×10^3 on GEODE, so at least one filter in every pair is overconfident by two orders of magnitude on Spires, without any reference to a gold standard. Table II reports the median over tracks of the per-track median with a 95% bootstrap interval over tracks, GEODE restricted to the tracks on which both filters of the pair converge. I2EKF-LO is omitted because it runs two iterated EKFs in place of an IMU and reports a covariance from each, so there is no single Σ to sum with a partner's. The bound holds under positively correlated errors; using the gold standard to check this hypothesis, the symmetric part of the estimated cross-covariance is positive semidefinite on 9 of the 10 Fast-LIO2–Faster-LIO tracks

(two of the twelve are excluded, Faster-LIO diverging) and on about half the tracks of the pairs involving Point-LIO. Where it fails, the worst direction inflates the numerator by at most $1.7\times$, which still leaves k_{pair} above 100. The result survives sweeping the clock offset up to $50\,\text{ms}$ and applying the full extrinsic, lever arm included. The k measured against the gold standard sits one to two orders of magnitude above the lower bound on Spires; the gap is either error common to the filters or error in the gold standard itself, and separating the two needs the gold standard's own covariance, which neither dataset ships.

B. The covariance ignores the residuals

The covariances of Table I are too tight by orders of magnitude, and the reason is structural. In the update step, the information added by a scan of N matched points is

$$\mathcal{J} = H_t^\top R^{-1} H_t = \sigma^{-2} \sum_{i=1}^{N} n_i n_i^\top,$$

with n_i the normals of the matched planes, at most one per voxel, and σ the configured measurement noise (Fig. 3b). We call $\mathcal{J}$ the credit, since it is the information the filter credits the scan with. The residuals, how far the scan lies off those planes, move the mean but do not enter $\mathcal{J}$. Since the n_i are unit vectors, $\operatorname{tr}\mathcal{J} = N/\sigma^2$, so the total information is fixed by the match count and the noise constant before the scan is compared to the map. Fast-LIO2 assigns $\sigma^2 = 10^{-3}\,\text{m}^2$ to each of $N \approx 5.7\times10^3$ matched points, which if spread evenly gives $0.7\,\text{mm}$ of standard deviation per axis, while the same track is accurate to $6\,\text{cm}$ (Fig. 1). The two numbers come from different sources, and nothing ties them together. This is why the overconfidence in Sect. IV-A does not respond to divergence or scene degeneracy. The covariance reflects the configuration, and the configuration does not change with the scene.

Sharpness is paid for in consistency: Figs. 3c and 3d sweep the measurement noise R and the voxel size of each filter, which together set the credited information, across 30 nats of precision on 23 tracks from Spires and GEODE. Proposition III.1 gives the sweep two predictions to choose between. If the sharpening is *earned*, the error shrinks with the covariance and the NEES holds, so the error falls 0.072 decades per nat of precision and the NEES is flat. If it is *unearned*, the error stays where it was and the median NEES rises 0.145 decades per nat. The four filters follow the 0.145 line across five orders of magnitude in NEES, with 22 of the 23 filter–scene tracks covering 0.145 in their 95% confidence interval. A 0.145 slope with the covariance's shape preserved means the error itself did not move, and Fig. 3d shows this directly. Point-LIO's steeper 0.207 on keble-college-02 is the exception, its error growing with the credit because it updates per point with a gain scaling as $1/R$; dividing out the measured error returns 0.141, so its covariance follows the configuration like the others. The sharpening is unearned. The credit computed from the normals and σ^2 alone matches the precision read off the filter's covariances to within 10^{-2} nats, so the configuration accounts for all of the reported precision.

TABLE II

PAIRWISE INFLATION PER FILTER PAIR.

Pair	k_{pair} ($\to$1)	
Oxford Spires		
Fast-LIO2 / Faster-LIO	3.2×10^2	$[1.4, 4.4]\times10^2$
Fast-LIO2 / Point-LIO	3.3×10^2	$[7.3, 82]\times10^1$
Faster-LIO / Point-LIO	1.8×10^2	$[5.2, 52]\times10^1$
GEODE converged		
Fast-LIO2 / Faster-LIO	5.8×10^3	$[4.1, 660]\times10^2$
Fast-LIO2 / Point-LIO	4×10^2	$[1.9, 348]\times10^1$
Faster-LIO / Point-LIO	1.5×10^1	$[0.81, 5.2]\times10^1$

The distance from a filter's median NEES down to the consistent value 2.37 is $3\ln k$ nats for the inflation k of Table I; on Spires k runs 5.7×10^2 to 6.7×10^6, so the filters sit 19 to 47 nats of precision above consistency. At a median NEES of 10^4 each further nat costs some 1.7×10^3 nats of log score, which is why the scores of Table I run to thousands. A filter that let its residuals inform its covariance, through a noise estimated from the innovations, a robust kernel, or an observability test, would take less of the credit as more is offered, and its NEES slope would fall below 0.145. None of the four does.

The dominant errors displace the whole scan together: The overcounting has a simple source, and the obvious fix does not remove it. Setting $R = \sigma^2 I$, as all four filters do, declares the N points of a scan to be N independent measurements, so the credit grows as N/σ^2. The errors that dominate a scan are not independent. Extrinsic calibration, the LiDAR–IMU time offset, motion distortion and drift in the map displace every point of the scan together, and each is one unknown rather than N. Sampling more points off the same surfaces cannot resolve a displacement they all share, so the information a scan carries saturates while the credit keeps growing. This holds for any likelihood that factorizes over the points, whatever residual it uses.

The obvious fix is to marginalize the shared displacement as a per-scan $\delta \sim \mathcal{N}(0, \Sigma_\delta)$, which gives $R = \sigma^2 I + H_t \Sigma_\delta H_t^\top$ and caps the credited information at $(\Sigma_\delta + \sigma^2 (H_t^\top H_t)^{-1})^{-1} \preceq \Sigma_\delta^{-1}$. We tested it post hoc on the Fast-LIO2 R sweep of Fig. 3c, where it fails. Applied at a single update it recovers 3.3 of the track's 23.7 nats, a step in the right direction but a small one. Applied at every update it does reach nominal, but only at $\Sigma_\delta^{1/2} = 1.1\,\text{m}$, $277\times$ the $4\,\text{mm}$ the innovation actually shows. A displacement that size is not one the scans have.

Marginalizing a shared displacement is therefore the right correction applied in the wrong place. What the points share is not drawn afresh each scan; it accumulates in the map, and the innovation, which measures a scan against that map, cannot see it. The uncertainty the filters are missing is the map's, and carrying it belongs to a different paper.

The likelihood offers two dials for handing back the 23.7 nats of keble-college-02, which runs on $N \approx 5.7\times10^3$ points. Inflating σ closes the gap only at $2\,\text{m}$ of assumed noise per point, two orders of magnitude above the sensor's ranging error. Discounting the count closes it at one or two

independent points per scan. Read this way, N/k is the scan's effective sample size, and the filters are running at k times it.

V. Limitations

Five limitations qualify the case study. Scoring first aligns the estimated track to the gold standard by a rigid transform, and that alignment is fitted to the same gold standard the scores then use. Fitting it over the whole track is the generous choice, and aligning on the first pose alone raises every median k further. The condition number κ is only a proxy for degeneracy, though for the two filters with accessible Jacobians every tested scalar summary of their information matrices explains as little. All four filters build on the iterated error-state Kalman filter, so the replication runs across implementations, sensors and datasets rather than across estimator architectures, with the smoother GLIM the one outside point. Consecutive errors are strongly dependent, with a lag-one autocorrelation near 0.99, so uncertainty attaches only at the track level. Finally, the inflation k is a median and $\mathrm{cov}_{0.9}$ is saturated at zero, so the two together characterize bulk inflation and the presence of unflagged large errors but not the magnitude of errors in the tail.

VI. Concluding remarks

Scoring the beliefs of four LiDAR-inertial filters over 67 tracks finds their reported covariances 2 to 7 orders of magnitude too tight, and set by the configuration rather than by the scene. Both findings are reproducible without a gold standard: the tightness by scoring two filters against each other, and the dependence on configuration by predicting the reported precision from the noise constant and the matched normals alone. Only the claim that the sharpening is unearned needs the reference. Point error alone would have shown none of this. Odometry that reports a belief should be scored as one, and to that end we release `smfeval`, an open-source implementation of the scores, tests, and intervals of this paper.

One choice in the methodology deserves more attention than it usually gets. An odometry filter leaves some degrees of freedom of its track unpinned, six for a LiDAR-only filter and four once an IMU fixes gravity, and scoring fits these to the gold standard before any score is computed. Every score is therefore conditional on that fit, and the fit uses the reference it is then judged against. The choice is not neutral. A whole-track SE(3) fit is the most generous, a first-pose fit the least, and an inertial filter fitted on six degrees of freedom has its pitch and roll corrected for free. In this study the gauge moves k_{pair} by under 5% on Spires and up to $2\times$ on GEODE, which is negligible against inflations of 10^2 to 10^6 but would decide the outcome for a well-calibrated filter. Two remedies follow. The estimator should declare its gauge rather than leave the evaluator to guess it, which `smfeval`'s format requires; and where a transform must be fitted, it should enter the belief as an uncertain quantity rather than a fixed correction, which needs a gold standard with its own covariance. Neither dataset supports the second yet.

We score translation only. Proper scores on SO(3) face intractable normalizers in the natural belief families, and supplying them is the next step.

Acknowledgments

This work was supported by the Danish Data Science Academy, which is funded by the Novo Nordisk Foundation (NNF21SA0069429). We used a generative language model for grammatical refinement, literature review assistance, and code debugging.

References

[1] T. Gneiting and A. E. Raftery, "Strictly proper scoring rules, prediction, and estimation," *J. Amer. Statist. Assoc.*, vol. 102, no. 477, pp. 359–378, 2007.

[2] M. Grupp, "evo: Python package for the evaluation of odometry and SLAM," https://github.com/MichaelGrupp/evo, 2017.

[3] H. R. Künsch, "The jackknife and the bootstrap for general stationary observations," *Ann. Statist.*, vol. 17, no. 3, pp. 1217–1241, 1989.

[4] D. N. Politis and H. White, "Automatic block-length selection for the dependent bootstrap," *Econom. Rev.*, vol. 23, no. 1, pp. 53–70, 2004.

[5] J. Sturm, N. Engelhard, F. Endres, W. Burgard, and D. Cremers, "A benchmark for the evaluation of RGB-D SLAM systems," in *Proc. IEEE/RSJ Int. Conf. Intell. Robots Syst. (IROS)*, 2012, pp. 573–580.

[6] Z. Zhang and D. Scaramuzza, "A tutorial on quantitative trajectory evaluation for visual(-inertial) odometry," in *Proc. IEEE/RSJ Int. Conf. Intell. Robots Syst. (IROS)*, 2018.

[7] ——, "Rethinking trajectory evaluation for SLAM: A probabilistic, continuous-time approach," in *Proc. ICRA Workshop Dataset Gener. Benchmarking SLAM Algorithms*, 2019.

[8] Y. Bar-Shalom, "On the track-to-track correlation problem," *IEEE Trans. Autom. Control*, vol. 26, no. 2, pp. 571–572, 1981.

[9] M. Joerger, F.-C. Chan, and B. Pervan, "Solution separation versus residual-based RAIM," *NAVIGATION: J. Inst. Navig.*, vol. 61, no. 4, 2014.

[10] S. J. Julier and J. K. Uhlmann, "A counter example to the theory of simultaneous localization and map building," in *Proc. IEEE Int. Conf. Robot. Autom. (ICRA)*, vol. 4, 2001, pp. 4238–4243.

[11] A. Censi, "An accurate closed-form estimate of ICP's covariance," in *Proc. IEEE Int. Conf. Robot. Autom. (ICRA)*, 2007.

[12] M. Brossard, S. Bonnabel, and A. Barrau, "A new approach to 3D ICP covariance estimation," *IEEE Robot. Autom. Lett.*, vol. 5, no. 2, 2020.

[13] J. M. Bernardo, "Expected information as expected utility," *Ann. Statist.*, pp. 686–690, 1979.

[14] Y. Bar-Shalom, X. R. Li, and T. Kirubarajan, *Estimation with Applications to Tracking and Navigation: Theory, Algorithms and Software*. John Wiley & Sons, 2001.

[15] T. Gneiting, F. Balabdaoui, and A. E. Raftery, "Probabilistic forecasts, calibration and sharpness," *J. Roy. Statist. Soc. B*, vol. 69, no. 2, pp. 243–268, 2007.

[16] B. Efron, "Bootstrap methods: another look at the jackknife," *Ann. Statist.*, vol. 7, no. 1, 1979.

[17] Y. Tao, M. Á. Muñoz-Bañón, L. Zhang, J. Wang, L. F. T. Fu, and M. Fallon, "The Oxford Spires dataset: Benchmarking large-scale LiDAR-visual localisation, reconstruction and radiance field methods," *Int. J. Robot. Res.*, 2024.

[18] Z. Chen, Y. Qi, D. Feng, X. Zhuang, H. Chen, X. Hu, J. Wu, K. Peng, and P. Lu, "Heterogeneous LiDAR dataset for benchmarking robust localization in diverse degenerate scenarios," *Int. J. Robot. Res.*, vol. 45, no. 1, pp. 6–22, 2026.

[19] W. Xu, Y. Cai, D. He, J. Lin, and F. Zhang, "FAST-LIO2: Fast direct LiDAR-inertial odometry," *IEEE Trans. Robot.*, vol. 38, no. 4, 2022.

[20] C. Bai, T. Xiao, Y. Chen, H. Wang, F. Zhang, and X. Gao, "Faster-LIO: Lightweight tightly coupled LiDAR-inertial odometry using parallel sparse incremental voxels," *IEEE Robot. Autom. Lett.*, vol. 7, no. 2, pp. 4861–4868, 2022.

[21] D. He, W. Xu, N. Chen, F. Kong, C. Yuan, and F. Zhang, "Point-LIO: Robust high-bandwidth light detection and ranging inertial odometry," *Adv. Intell. Syst.*, vol. 5, no. 7, p. 2200459, 2023.

[22] W. Yu, J. Xu, C. Zhao, L. Zhao, T.-M. Nguyen, S. Yuan, M. Bai, and L. Xie, "I^{2}EKF-LO: A dual-iteration extended Kalman filter based LiDAR odometry," in *Proc. IEEE/RSJ Int. Conf. Intell. Robots Syst. (IROS)*, 2024, pp. 10 453–10 460.

[23] K. Koide, M. Yokozuka, S. Oishi, and A. Banno, "GLIM: 3D range-inertial localization and mapping with GPU-accelerated scan matching factors," *Robot. Auton. Syst.*, vol. 179, p. 104750, 2024.

[24] I. Vizzo, T. Guadagnino, B. Mersch, L. Wiesmann, J. Behley, and C. Stachniss, "KISS-ICP: In defense of point-to-point ICP — simple, accurate, and robust registration if done the right way," *IEEE Robot. Autom. Lett.*, vol. 8, no. 2, pp. 1029–1036, 2023.

[25] D. He, W. Xu, and F. Zhang, "Kalman filters on differentiable manifolds," 2021, arXiv:2102.03804, unpublished.